

tionary density perturbations can be established by a beam-driven pump wave with finite k_0 at $\omega \sim \omega_p$, (2) the localization of field arises from the nonlinear development of the stationary instability, and (3) the localized intense fields can be responsible for the generation of high-energy electrons in electron-beam-plasma interactions.

We wish to acknowledge valuable discussions with Professor J. M. Dawson, Professor B. Fried, Professor G. Morales, Professor Y. C. Lee, and Dr. J. Drake. The technical assistance of Z. Lucky is greatly appreciated.

*Research supported by the National Science Foundation under Grant No. NSF GP 38673X2.

¹H. C. Kim, R. Stenzel, and A. Y. Wong, *Phys. Rev. Lett.* **33**, 886 (1974), have demonstrated the strong localization of fields in a nonuniform plasma at the cut-off region $\omega_{pe}(x) \sim \omega_0$, where ω_0 is the frequency of the

external quasistatic field.

²K. Nishikawa, *J. Phys. Soc. Jpn.* **24**, 916, 1152, (1968).

³V. E. Zakharov, *Zh. Eksp. Teor. Fiz.* **62**, 1745 (1972) [*Sov. Phys. JETP* **35**, 908 (1972)].

⁴A. S. Kingsep, L. I. Rudakov, and R. N. Sudan, *Phys. Rev. Lett.* **31**, 1482 (1973); G. Morales and Y. C. Lee, *Phys. Rev. Lett.* **33**, 1534 (1974); E. J. Valeo and W. L. Kruer, *Phys. Rev. Lett.* **33**, 750 (1974); G. J. Morales, Y. C. Lee, and R. B. White, *Phys. Rev. Lett.* **32**, 457 (1974); L. Thode and R. N. Sudan, *Phys. Rev. Lett.* **30**, 732 (1973).

⁵B. H. Quon, A. Y. Wong, and B. H. Ripin, *Phys. Rev. Lett.* **32**, 406 (1974).

⁶T. M. O'Neil and J. H. Malmberg, *Phys. Fluids* **11**, 754 (1968).

⁷The ion-density perturbation is observed to persist for 20–30 μ sec after the pump wave is turned off.

⁸A. Y. Wong and G. Schmidt, University of California at Los Angeles Plasma Physics Group Report No. 151, 1973 (unpublished).

⁹R. Z. Sagdeev and A. A. Galeev, *Nonlinear Plasma Theory* (Benjamin, New York, 1969).

Superconductivity in Dilute Alloys of TaS₂ with Fe[†]*

Robert M. Fleming and R. V. Coleman

Department of Physics, University of Virginia, Charlottesville, Virginia 22901

(Received 11 March 1975)

Single crystals of iron-doped TaS₂ grown from sintered powders of composition Fe_{0.05}-TaS₂ show a rise in critical temperature to above 3 K and an enhanced anisotropy of H_{c2} which is comparable to that observed in 2H-TaS₂(pyridine)_{1/2}. Single crystals grown from Fe_{0.05}T_{0.95}S₂ powders are stabilized in the 1T phase and are semiconducting at all temperatures below room temperature with no resistive anomaly at 200 K.

Dilute concentrations of Fe in TaS₂ produce major changes in both the superconducting and normal phases of this layer structure. The results suggest that the electronic and crystal structure is extremely sensitive to the way in which iron is incorporated into the crystal. Previous results on Fe_xNbSe₂ single crystals¹ and powders² have shown a rapid quenching of the superconducting transition. In addition the single crystals¹ of Fe_xNbSe₂ show a strong resistivity minimum in the range 10 to 15 K. Single crystals of Fe_xTaSe₂ also show a strong resistance minimum as well as evidence for magnetic behavior of the iron impurities, and this data will be presented in a later paper. The behavior of Fe_xTaS₂ is quite different and initial results on these alloys as well as dilute alloys of composi-

tion Fe_xTa_{1-x}S₂ are presented below.

Single crystals have been grown by two methods. In one case an intercalation alloy is produced by sintering additional Fe with stoichiometric amounts of Ta and S to give a compound Fe_xTaS₂ where x ranged from 0–10 at.% and corresponds to excess metal ions. In the second case Fe was mixed with Ta and S to give an alloy Fe_xTa_{1-x}S₂ where the total metal ion content is stoichiometric with S. Single crystals were grown from the sintered materials by iodine-vapor transport. Mass spectrographic analysis has shown that the iron content of the single crystal is practically identical to that of the initial sintered powder. A comparison of iron spectral line intensities for a powder and the resulting single crystal of Fe_{0.05}TaS₂ is shown in the inset

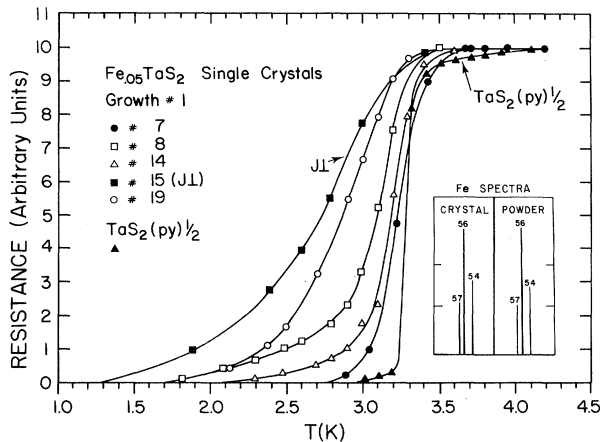


FIG. 1. Superconducting to normal state transitions measured in a resistance versus temperature experiment. Transition in $\text{Fe}_{0.05}\text{TaS}_2$ and in $2H\text{-TaS}_2(\text{pyridine})_{1/2}$. Inset shows comparison of mass spectrograph lines for iron isotopes 54, 56, and 57 in powder and single crystal of $\text{Fe}_{0.05}\text{TaS}_2$.

of Fig. 1. The analysis also indicates little or no loss of Ta or S during the transport process. X-ray powder patterns for the sintered powders show the $\text{Fe}_{0.05}\text{Ta}_{0.95}\text{S}_2$ to be in the $1T$ phase while the $\text{Fe}_{0.05}\text{TaS}_2$ sintered powder is predominantly in the $2H$ phase. The electronic properties and crystal phases obtained by the two methods are completely different and in this Letter we report initial measurements of the electronic behavior using resistance and magnetoresistance methods.

For the alloys with excess metal, addition of iron steadily increases the transition temperature of the $2H$ phase to a maximum of ~ 3.5 K corresponding to approximately 5 at.% iron. The superconducting transition is completely suppressed in powders only after the addition of ~ 10 at.% iron. For the higher excess-iron concentrations nearly perfect small crystals of a second phase form in the growth chamber and these do not transform during cooling. The electronic properties of this phase will be reported later.

For the substitutional iron alloy, 5 at.% Fe is sufficient to stabilize the $1T$ phase at all temperatures below the growth temperature and produces shiny gold-tinted single-phase crystals as checked by x-ray diffraction. Reheating and cooling has no effect on these crystals which are completely stable at all temperatures below the growth temperature. They are semiconducting in the temperature range 1–300 K, but show no

sharp resistive transition as is observed³ in pure $1T\text{-TaS}_2$ at ~ 200 K.

We first discuss the superconducting properties of the intercalation alloys. In this case the alloy appears to grow in the $1T$ phase and transform to the $2H$ phase during cooling from the growth temperature in the same way as observed for pure TaS_2 . These crystals remain in the shiny gold-tinted $1T$ phase when quenched from the growth temperature. Reheating and slow cooling will transform them into the low-temperature $2H$ phase showing the high T_c and critical-field anisotropy. The iron is thought to enter the octahedral holes between the prismatic layers of TaS_2 as Fe^{2+} ions although this has been established in detail⁴ only for much more concentrated intercalation alloys in powder form. Figure 1 shows resistive transitions for five single crystals of $\text{Fe}_{0.05}\text{TaS}_2$ from a given growth. Selected crystals show transitions comparable to those observed in well-intercalated $2H\text{-TaS}_2(\text{pyridine})_{1/2}$ crystals^{5,6} and data for a pyridine-intercalated crystal are also shown in Fig. 1.

The $\text{Fe}_{0.05}\text{TaS}_2$ single crystals show a greatly enhanced anisotropy of H_{c2} which is comparable to that observed in $\text{TaS}_2(\text{pyridine})_{1/2}$ and Figs. 2(a) and 2(b) show the critical-field anisotropy observed for $\text{Fe}_{0.05}\text{TaS}_2$ and $\text{TaS}_2(\text{pyridine})_{1/2}$ for angles of H between 0 and 10° relative to the orientation parallel to the layers. The critical-field anisotropy was first treated by Lawrence and Doniach⁷ and by Kats⁸ using anisotropic Ginzburg-Landau equations with a Josephson coupling between the layers. Such models lead to a useful representation for the angular dependence of the form $[H_{c2}(\theta)]^2/[H_{c2}(90^\circ)]^2 = 1/(\sin^2\theta + \epsilon^2 \cos^2\theta)$, where ϵ^2 is the Ginzburg-Landau anisotropic mass ratio m/M . Data for $\text{Fe}_{0.05}\text{TaS}_2$ and $2H\text{-TaS}_2(\text{pyridine})_{1/2}$ are fitted with this model by the dashed lines in Fig. 2 and give values of $1/\epsilon^2 = M/m > 400$ which is ten times larger than observed for pure $2H\text{-TaS}_2$ ($M/m \approx 45$) [see lower curve of Fig. 2(b)].

Klemm, Luther, and Beasley⁹ and Bulaevskii¹⁰ have recently examined the upper critical field of layer structures in much greater detail. Bulaevskii¹⁰ has given an expression for the critical-field anisotropy for temperatures close to T_c where the normal to superconducting transition is second order and this is given below.

$$\frac{H_{c2}^2(\theta)}{H_{c2}^2(1)} = \frac{1 + 2x^2 - (1 + 4x^2)^{1/2}}{2x^4 \sin^2\theta}, \quad (1)$$

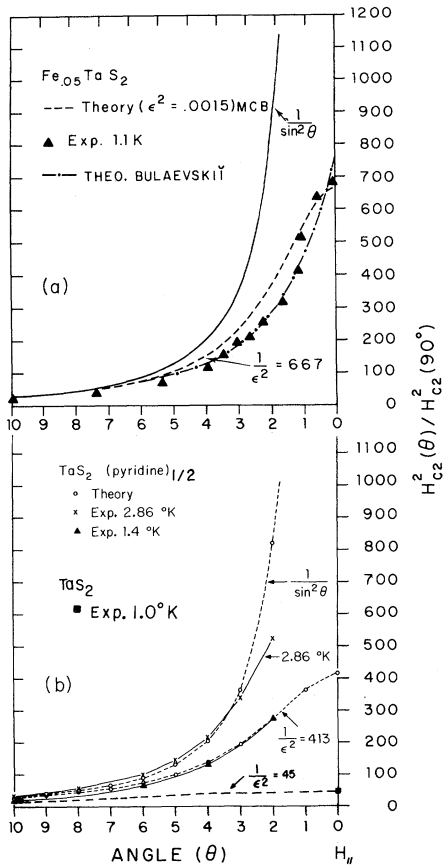


FIG. 2. Angular dependence of critical field $H_{c2}(\theta)$ as a function of angle measured from H parallel to the layers. The ratio $[H_{c2}(\theta)]^2/[H_{c2}(90^\circ)]^2$ is plotted over the range 1° – 10° . Dashed curves represent the function $1/[\sin^2\theta + \epsilon^2 \cos^2\theta]$. (a) Data for $\text{Fe}_{0.05}\text{TaS}_2$ at 1.1 K and fit by formula (1). (b) Data for $2H\text{-TaS}_2$ at 1.0 K and $2H\text{-TaS}_2(\text{pyridine})_{1/2}$ at 2.86 and 1.4 K.

where

$$x = \frac{H_{c2}(\perp)}{H_{c2}(\parallel) \sin\theta} \text{ and } H_{c2}(\parallel) = \frac{2\pi T_c (1-t)^{1/2}}{\mu_0 [7\zeta(3)]^{1/2}};$$

$\mu_0 = g\mu_B/2$ and $\zeta(3)$ is the Reimann ζ function.

The data on $\text{TaS}_2(\text{py})_{1/2}$ in Fig. 2(b) for $T = 2.86$ K ($t = T/T_c = 0.88$) are fit very well by this expression with the correct T_c and ratio $H_{c2}(\perp)/H_{c2}(\parallel)$ (see details in Ref. 10). The data at 1.4 K ($t = 0.43$) were taken later and the resistivity of the pyridine-intercalated sample had increased from $\rho_{\parallel} = 10^{-5} \Omega \text{ cm}$ to $\rho_{\parallel} = 6 \times 10^{-5} \Omega \text{ cm}$ observed for the $\text{Fe}_{0.05}\text{TaS}_2$ crystal used for the data in Fig. 2(a). These crystals are closer to the dirty limit and values of $H_{c2}(\theta)$ calculated from expression (1) with all parameters determined from experiment are lower than observed. However, with x

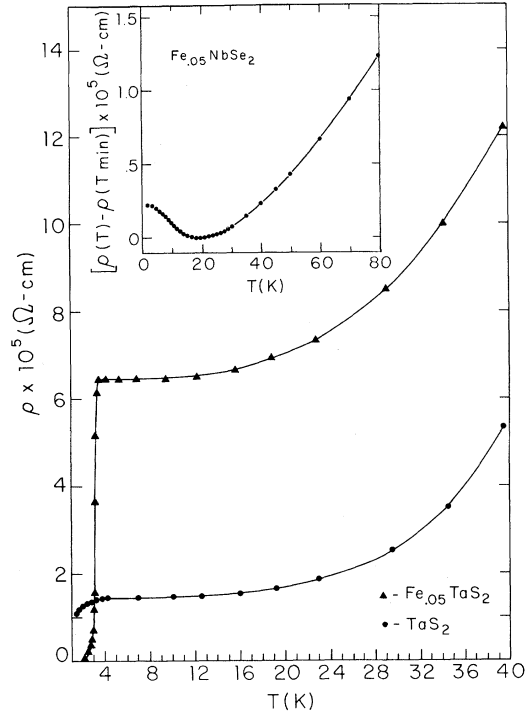


FIG. 3. Temperature dependence of parallel resistivity for $\text{Fe}_{0.05}\text{TaS}_2$, $\text{Fe}_{0.05}\text{NbSe}_2$, and pure $2H\text{-TaS}_2$ in the range 1–40 K.

treated as an adjustable parameter expression (1) can be fitted quite well to the angular data as shown in Fig. 2(a) and the resulting value of x is in agreement with the observed ratio $H_{c2}(\perp)/H_{c2}(\parallel)$.

The temperature dependence of resistance for $\text{Fe}_{0.05}\text{TaS}_2$ is shown in Fig. 3 and no resistance minimum is observed in contrast to the results for $\text{Fe}_{0.05}\text{NbSe}_2$ and $\text{Fe}_{0.05}\text{TaSe}_2$ (see inset in Fig. 3). The resistance minimum in $\text{Fe}_{0.05}\text{NbSe}_2$ is field dependent and highly anisotropic¹ and no such effects are observed in $\text{Fe}_{0.05}\text{TaS}_2$ indicating that the Fe in $2H\text{-TaS}_2$ up to at least 5-at.% excess exhibits no magnetic character in contrast to excess Fe in NbSe_2 and TaSe_2 . The enhanced superconductivity and anisotropy in Fe_xTaS_2 indicates an effective decoupling of the layers. This would require the iron to be very effective in breaking the superconducting pairs moving perpendicular to the layers. This could be accomplished by strong interaction with iron impurities between the layers or by some more complex phase modification in which alternating sandwiches show strong superconductivity and are weakly coupled across layers modified by the iron. Such

a phase would be similar in behavior to the pure $4Hb$ - TaS_2 phase where alternating metallic and semiconducting layers exist¹¹ in the normal phase. The initial measurements of $\rho_{\perp}/\rho_{\parallel}$ for $Fe_{0.05}TaS_2$ above T_c at 4.2 K show values ≥ 1000 and these are comparable to the ratios observed for $4Hb$ - TaS_2 by DiSalvo *et al.*¹¹ in the helium-temperature range.

When the Fe is added substitutionally for the Ta the resulting alloy $Fe_{0.05}T_{0.95}S_2$ appears to entirely stabilize in the $1T$ phase. No crystallographic phase transition occurs on cooling from the growth temperature and the resistivity shows semiconducting behavior down to 1 K with no evidence of the transition anomaly at 200 K (see Fig. 4). Wilson, DiSalvo, and Mahajan¹² have extensively discussed the formation of charge-density waves (CDW) particularly in the $1T$ phases of these materials. In general substitutional impurities tend to suppress the commensurate CDW temperature and reduce the amplitude of the CDW. In Ref. 12, in fact, it was found that $\frac{1}{2}$ at.% substitutional Ti in TaS_2 also completely removes the 200-K transition in $1T$ - TaS_2 .

In the $2H$ or $4Hb$ phases the CDW's generally have lower amplitude and a more complex behavior, but could certainly have effects on the superconducting transition. Morris¹³ has suggested on the basis of Hall-effect measurements that suppression of the CDW in $2H$ - $NbSe_2$ by Fe

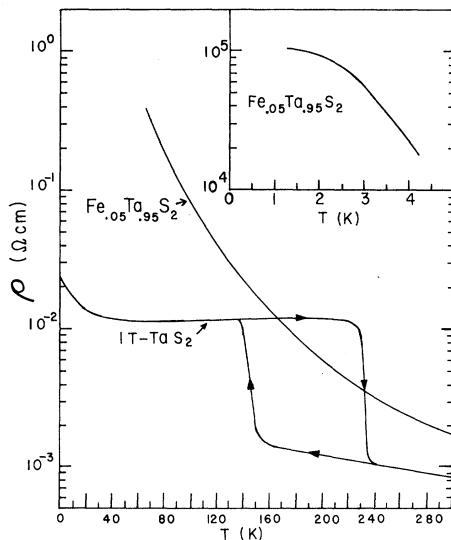


FIG. 4. Temperature dependence of parallel resistivity for $Fe_{0.05}T_{0.95}S_2$ in the range 1–300 K. Resistivity versus temperature for pure $1T$ - TaS_2 is also shown from Ref. 8.

or Mn correlates with the suppression of T_c in this material. In the present case of enhancement of T_c by Fe it would be interesting to explore a possible relation between the CDW and the increase of T_c and more experiments will be required on these interesting systems.

The authors would like to acknowledge the contribution of Professor R. C. Morris who participated in some phases of the work. Estelle Phillips has assisted in sample preparation and measurements. Useful discussions have been held with Professor J. Ruvalds and Professor V. Celli. Professor W. Harrison and Professor K. Lawless have aided in the x-ray and mass spectrograph work.

† Work supported by the U. S. Atomic Energy Commission Contract No. AT-(40-1)-3105.

*Work above 80 kOe was performed while the authors were Guest Scientists at the Francis Bitter National Magnet Laboratory, which is supported at the Massachusetts Institute of Technology by the National Science Foundation.

¹R. C. Morris, B. W. Young, and R. V. Coleman, in *Magnetism and Magnetic Materials—1973*, AIP Conference Proceedings No. 18, edited by C. D. Graham, Jr., and J. J. Rhyne (American Institute of Physics, New York, 1974), p. 292.

²J. J. Hauser, M. Robbins, and F. J. DiSalvo, *Phys. Rev. B* **8**, 1038 (1973).

³A. H. Thompson, F. R. Gamble, and J. F. Revelli, *Solid State Commun.* **9**, 981 (1971).

⁴K. Anzenhafer, J. M. Van Den Berg, P. Cossee, and J. N. Helle, *J. Phys. Chem. Solids* **31**, 1057 (1970).

⁵F. R. Gamble, F. J. DiSalvo, R. A. Klemm, and T. H. Geballe, *Science* **168**, 568 (1970).

⁶R. C. Morris and R. V. Coleman, *Phys. Rev. B* **7**, 991 (1973).

⁷W. E. Lawrence and S. Doniach, in *Proceedings of the Twelfth International Conference on Low Temperature Physics, Kyoto, 1970*, edited by E. Kanda (Keigaku Publishing Co., Tokyo, 1971), p. 361.

⁸E. I. Kats, *Zh. Eksp. Teor. Fiz.* **56**, 1675 (1969) [*Sov. Phys. JETP* **29**, 897 (1969)], and **58**, 1471 (1970) **31**, 787 (1970).

⁹R. A. Klemm, A. Luther, and M. R. Beasley, to be published.

¹⁰L. N. Bulaevskii, *Zh. Eksp. Teor. Fiz.* **65**, 1278 (1973) [*Sov. Phys. JETP* **38**, 634 (1974)].

¹¹F. J. DiSalvo, B. G. Bagley, J. M. Voorhoeve, and J. V. Waszczak, *J. Phys. Chem. Solids* **34**, 1357 (1973).

¹²J. A. Wilson, F. J. DiSalvo, and S. Mahajan, *Advan. Phys.* **24**, 117 (1975), and *Phys. Rev. Lett.* **32**, 882 (1974).

¹³R. C. Morris, *Phys. Rev. Lett.* **34**, 1164 (1975).